



Gypenoside GP5 effectively controls *Colletotrichum gloeosporioides*, an anthracnose fungus, by activating autophagy

Yujie Liu^a, Xinyv Li^{a,b}, Chu Gong^a, Yonghong Cao^d, Jun Wang^{a,*}, Min Han^{e,*}, Jun-Li Yang^{c,*}

^a Shandong Laboratory of Advanced Materials and Green Manufacturing at Yantai, Yantai 264000, China

^b Qingdao Agricultural University, College of Food Science and Engineering, Qingdao 266109, China

^c CAS Key Laboratory of Chemistry of Northwestern Plant Resources and Key Laboratory of Natural Medicine of Gansu Province, Lanzhou Institute of Chemical Physics, Chinese Academy of Sciences (CAS), Lanzhou 730000, China

^d Zanthoxylum Bungeanum Research Institute, Longnan Economic Forest Research Institute, Longnan 746000, China

^e Department of Stomatology, The First Affiliated Hospital of Shandong First Medical University & Shandong Provincial Qianfoshan Hospital, Jinan 250014, China

ARTICLE INFO

Keywords:

Colletotrichum gloeosporioides
Gynostemma pentaphyllum (Thunb.) Makino
Gypenosides
Autophagy

ABSTRACT

Anthracnose is a plant disease caused by *Colletotrichum spp.*, known for its widespread infectivity and extreme destructiveness. *Colletotrichum gloeosporioides* is a representative pathogen of anthracnose in China. Gypenosides GP4-GP7, derived from *Gynostemma pentaphyllum* (Thunb.) Makino, could significantly inhibit the growth of *C. gloeosporioides* mycelial, with EC₅₀ values of 96.98, 27.5, 38.48, and 61.59 mg L⁻¹. The inhibitory effect of these compounds surpassed the commonly used chemical pesticide chlorothalonant and plant-derived pesticide matrine. Among them, the most active compound GP5 also showed a significant inhibitory effect on spore germination and bud tube elongation of *C. gloeosporioides*. In addition, GP5 could effectively suppress the spread of anthracnose spots in postharvest fruit. Transmission electron microscopy and fluorescence microscopy demonstrated that GP5 primarily exerted its antifungal function by activating cellular autophagy. Additionally, proteomics analysis revealed that GP5 had an antifungal effect against *C. gloeosporioides* by enhancing cellular autophagy through upregulation of the expression of the autophagy-related protein Atg8. This study presents a novel approach for the control and management of anthracnose in *C. gloeosporioides*. Consequently, GP5 has the potential to be developed as a plant-derived fungicide for the biological control of anthracnose.

1. Introduction

Anthracnose, caused by *Colletotrichum spp.*, is one of the most urgent worldwide plant diseases. *Colletotrichum spp.* ranks one of the top ten plant pathogenic fungi, with strong destructiveness, wide distribution, and wide infection range (De Silva et al., 2017; Dean et al., 2012). *Colletotrichum spp.* mainly uses biotrophic and necrotrophic strategies to infect crops at various growth and development stages (De Silva et al., 2017; Health et al., 2022), especially near mature fruit. This leads to serious postharvest decay and economic losses of at least tens of billions of dollars annually (Wu et al., 2023). 280 kinds of *Colletotrichum spp.* are reported worldwide, and 139 kinds in China (Liu et al., 2022). Among them, *C. gloeosporioides* is a common pathogen in China, and it is also one of the most extensive host species and most harmful species in the world (Liu et al., 2022).

Chemical fungicides, such as prochloraz and difenoconazole (Zhang et al., 2023a), are still the primary methods to prevent and control anthracnose at present, but the problems caused by the abuse of chemical fungicides such as pathogen resistance, environmental pollution, food security, and so on need to be solved (Cheng et al., 2022; Do et al., 2021). Plants are a treasure house of natural antifungal substances. Compared with chemical fungicides, plant-derived fungicides developed using these active substances have the advantages of strong selectivity, relative safety to non-target organisms, and environmental friendliness. Therefore, further exploring the new alternative strategies using plant-derived active substances to control anthracnose is promising.

Gynostemma pentaphyllum (Thunb.) Makino, a member of the Cucurbitaceae family and commonly referred to as “jiaogulan” in China, is mainly distributed in China, Korea, Japan, and Southeast Asian

* Corresponding authors.

E-mail addresses: 18435996332@163.com (Y. Liu), LiXinyv0624@163.com (X. Li), GongChu@amgm.ac.cn (C. Gong), hongyongcao870405@163.com (Y. Cao), licpwangjun@163.com (J. Wang), 1894@sdhospital.com.cn (M. Han), yangjl@licp.cas.cn (J.-L. Yang).

<https://doi.org/10.1016/j.postharvbio.2024.113305>

Received 19 August 2024; Received in revised form 31 October 2024; Accepted 5 November 2024

Available online 16 November 2024

0925-5214/© 2024 Elsevier B.V. All rights are reserved, including those for text and data mining, AI training, and similar technologies.

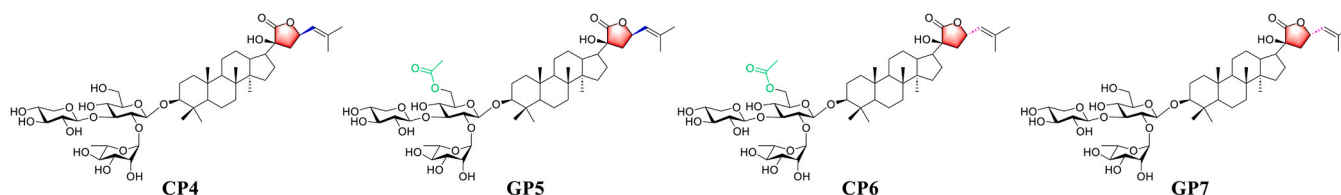


Fig. 1. Chemical structures of the compounds GP4-GP7.

countries (Tsang et al., 2019), known for its medicinal and health-protective affection for a long history in our country. Previous explorations of this plant entity have unveiled an intriguing range of gypenosides associated with its pharmacological properties. Gypenosides, belonging to dammarane-type saponins, impart a distinctive pharmacological fingerprint to *G. pentaphyllum*, elevating its significance in medicinal research. Previous investigations have demonstrated extensive pharmacological effects of gypenosides, including anti-cancer (Lu et al., 2017; Xing et al., 2019; Zhang et al., 2015), neuroprotective (Geng et al., 2022a; Geng et al., 2022b; Wang et al., 2019; Wang et al., 2022a; Wang et al., 2020; Zhai et al., 2021), and cardiovascular protection (Yu et al., 2016). We sought to illustrate the bioactive properties of gypenosides, with a focus on investigating their relatively unexplored potential as plant fungicides.

In the early stage, our research team systematically studied the chemical composition and biological activity of *G. pentaphyllum*. Several gypenosides and their derivatives were isolated, including 19 undescribed compounds (Wang et al., 2019; Wang et al., 2022b; Wang et al., 2017b; Wang et al., 2020). Previous studies have found that gypenosides GP4-GP7 (Fig. 1) with 20,23-dihydroxydammar-24-en-21-oic acid-21, 23-lactone nuclei were found to possess anti-*C. gloeosporioides* activities. Herein reported were the results of the activity and mechanism of gypenosides GP4-GP7 against *C. gloeosporioides*. This study provided a theoretical basis for the further development and utilization of *G. pentaphyllum* in agriculture. The detailed procedures have been described in the following sections.

2. Materials and methods

2.1. Reagent

GP4-GP7 were isolated from *G. pentaphyllum*. They were then dissolved in methanol as a mother liquor with a concentration of 40 g L⁻¹ and stored in 4 °C.

Acridine orange (AO) was purchased from Aladdin Reagent Co., Ltd. (Shanghai, China). Fluo-8, AM Ca²⁺ fluorescent probe was obtained from Applygen GO., Ltd. (Beijing, China). JC-1 kit was provided by Nanjing Jiancheng Bioengineering Institute (Nanjing, China).

2.2. Pathogen culture

C. gloeosporioides (CFCC 82113), which was obtained from the China Forestry Culture Collection Center, was isolated from a tomato plant at Laiyang Agricultural College in Shandong province. The fungus was activated by potato dextrose broth (PDB), and stored in glycerol.

2.3. Fruit

Apples (*Malus domestica* Borkh. cv. Red Fuji), grapes (*Vitis labrusca*×*vinifera*, 'Shine Muscat') and tomatoes (*Solanum lycopersicum* Mill.) with uniform maturity and size were harvested in Yantai bajiao farmer's market, Shandong province. The apples had a circumference of approximately 25–27 cm and weighed around 200–210 g. The grapes had an equatorial circumference of about 9–10 cm and weighed approximately 11–13 g. The tomatoes had an equatorial circumference of about 20–23 cm and weighed approximately 160–165 g. The fruit

were then immediately transported to the laboratory.

2.4. In vitro experiments with GP5 inhibition of *C. gloeosporioides*

The objective of the study was to investigate the inhibitory effect of compounds GP4-GP7 on the mycelial growth of *C. gloeosporioides* using the mycelial growth rate method (Wu et al., 2023). A volume of 1 mL of the glycerol reservoir was inoculated in 100 mL of PDB and incubated at 28 °C for 5 d. The fungal liquid was collected after filtration through sterile gauze. Spores were quantified using a hemocytometer, with the spore concentration in the experiment being 10⁶ spores mL⁻¹. A volume of 200 μL of the spore suspension was applied to a Petri dish (90 mm diameter) containing PDA (20 mL). The dishes were then incubated at 28 °C for 5 d to allow the formation of a fungal colony. GP4-GP7 were incorporated into PDA at concentrations of 12.5, 25, 50, 100, and 200 mg L⁻¹, respectively. A 6 mm diameter hole was created in the solid medium using a punch. And the 6 mm fungal colonies were carefully transferred to the solid media using sterile forceps. Petri dishes without any compounds were utilized as blank controls, while chlorothalonil and matrine were employed as positive controls. The above Petri dishes were placed in a 28 °C incubator, and each group was replicated three times.

2.5. Inhibition of GP5 on spore germination of *C. gloeosporioides*

Microscopic observation was employed to investigate the impact of GP5 on spore germination and bud tube elongation (Qiao et al., 2022). A spore suspension, containing 10⁶ spores mL⁻¹ and compound GP5 at EC₅₀ or 400 mg L⁻¹, was introduced into the PDB medium. The mixture was subsequently placed in a thermostatic incubator and incubated at 28 °C. The germination status of the spores was monitored using microscopy at 2 h intervals.

2.6. In vivo experiments with GP5 inhibition of *C. gloeosporioides*

Fruit acupuncture was conducted to investigate whether GP5 was applied to the fruit as a measure against anthrax (Hu et al., 2023). Fruit of uniform size, hardness, and skin color were selected and air-dried naturally after being washed with clean water. Following disinfection of the fruit surface with a 75 % ethanol spray, a sterile steel needle was used to create a trauma hole with a diameter and depth of 3 mm. Then, a 10 μL spore suspension was inoculated in the wound area, and various concentrations of GP5 (50, 500, 100 mg L⁻¹) were added after allowing it to naturally dry on the ultra-clean table. After air drying the wound surface, the fruit was placed in a fruit frame, sealed with plastic wrap, and placed in a constant temperature and humidity incubator.

2.7. Mycelial morphology and intracellular structural changes

2.7.1. Scanning electron microscopy (SEM)

Mycelial morphology was observed using SEM (Yang et al., 2023). Initially, a spore suspension of 300 μL was added to 30 mL of liquid medium PDB and incubated at a constant temperature of 28 °C. GP5 was then added to achieve a compound concentration of EC₅₀ and 400 mg L⁻¹. After 2 d of incubation, the mycelia were harvested and washed twice with PBS buffer. Subsequently, glutaraldehyde was added for overnight fixation. The washed mycelium was eluted in a gradient

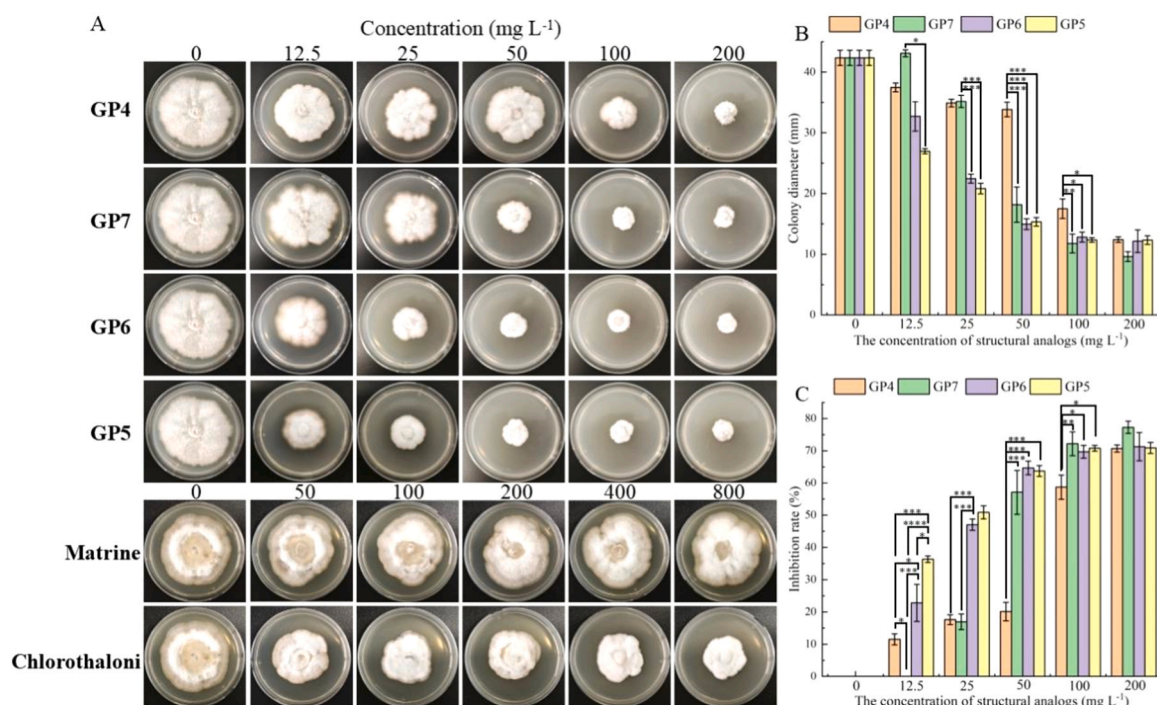


Fig. 2. Effect of GP5 and its structural similarity compounds on mycelial growth of *C. gloeosporioides*. (A) Effect of compounds on mycelial growth at different concentrations. (B) The colony diameter of *C. gloeosporioides* was measured after the addition of various concentrations of compounds. (C) The mycelial inhibition of *C. gloeosporioides* was observed at different concentrations of the compounds. Vertical bars represent standard deviations of the means, $n=3$. Asterisks denote significant differences, * $P < 0.05$, ** $P < 0.01$, *** $P < 0.001$, **** $P < 0.0001$.

using ethanol concentrations of 30 %, 50 %, 70 %, 90 %, and 100 %. The treated mycelium was frozen in the refrigerator for 2 h and then lyophilized for 4 h. The lyophilized mycelium was affixed to the sample table using conductive tape, and the morphology of the mycelium was observed using SEM.

2.7.2. Transmission electron microscopy (TEM)

To investigate the impact of GP5 on the organelle structure within the mycelial of *C. gloeosporioides*, as well as the alterations in the cell wall and cell membrane, TEM was employed for observation (Zhang et al., 2023b). The preprocessing of TEM was conducted in the same manner as that of SEM. Treated mycelial cells were fixed using a 2.5 % glutaraldehyde solution, washed three times with 1 mL of PBS solution, fixed again with a 1 % osmium acid solution, and ultimately dehydrated using various concentrations of ethanol. The mycelial cells were then permeabilized with white resin and samples were cut into thin sections for TEM observation.

2.8. Autophagy-related assays

Autophagy was visualized using AO staining, following previously established experimental protocols (Deng et al., 2024). The GP5 of the *C. gloeosporioides* was treated with a concentration of 400 mg L⁻¹, collected for a duration of 2 d, and washed twice with PBS buffer. The mycelium was incubated with a concentration of 1 μg mL⁻¹ AO in the dark at a temperature of 37 °C for a duration of 20 min. Subsequently, the mycelium was washed three times with PBS and observed using a Leica DM3000 microscope equipped with a blue-green laser (excitation wavelengths of 460–495 nm and 530–550 nm, and emission wavelengths of 505 nm and 570 nm).

2.9. Detection of the intracellular calcium ion (Ca²⁺) concentration

Cellular Ca²⁺ concentration was determined using the Fluo-8, AM Ca²⁺ fluorescent probe, following the instructions provided in the

experimental procedure reference kit (Yang et al., 2024). To initiate the experiment, 1 g of mycelial (wet weight) was added to 100 mL of PDB medium and GP5 at a concentration of 400 mg L⁻¹. The medium without GP5 was used as a blank control group and incubated in a constant temperature oscillation chamber for 2 d. The supernatant was removed by centrifugation and the mycelial were washed twice with PBS buffer. The medium was discarded and 100 μL of Fluo-8, AM working solution was added to cover the mycelial, which were then incubated at either 37 °C or room temperature for 0.5 h. The mycelial were subsequently washed twice with dilution buffer and visualized using fluorescence microscopy.

2.10. Mitochondrial membrane potential detection

Mitochondrial membrane potential changes were detected using the JC-1 kit, following the experimental procedure outlined in the kit instructions (Wang et al., 2023). Initially, 300 μL of spore suspension was added to 30 mL of PDB liquid medium and cultured at a constant temperature of 28 °C for 5 d. After centrifugation, 1 g of mycelial (wet weight) was added to 100 mL of PDB medium, with a GP5 concentration of EC₅₀ and 400 mg L⁻¹. The medium without GP5 was used as a control group and incubated in a constant temperature oscillation chamber for 2 d. The supernatant was removed by centrifugation and the mycelial were washed twice with PBS buffer. The mycelium was then evenly suspended in 500 μL of JC-1 staining solution and incubated at 37 °C in light for 20 min. The mycelium was collected by centrifugation (420 g, 5 min) at room temperature and rinsed twice with Incubation Buffer. Finally, the cells were re-suspended in 500 μL and visualized using a fluorescence microscope.

2.11. Proteomic analysis

The study conducted by Wang et al. (2021) focused on the protein expression of GP5 treatment using non-labeled quantitative proteomics. The proteomics experiments involved several steps, including protein

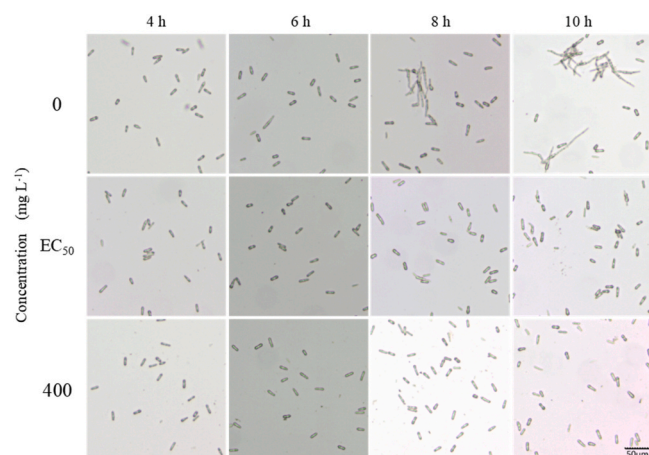


Fig. 3. Spore germination and bud tube length after GP5 treatment with EC₅₀ and 400 mg L⁻¹ concentration.

extraction, protein quantification, protein enzymatic hydrolysis, LC-MS/MS analysis, database retrieval, and data analysis. Initially, the supernatant was removed from each sample after treatment with an appropriate amount of SDT lysate. Protein quantification was then performed using the BCA method. Subsequently, an adequate quantity of protein from each sample was digested using the Filter-Aided Sample Preparation (FASP) method. The resulting peptides were purified through desalting using a C18 Cartridge and dried under vacuum conditions through lyophilization. The enzymatic peptides were further dried and reconstituted with 0.1 % FA for peptide concentration determination for LC-MS analysis. For separation and analysis, an appropriate amount of peptides was taken from each sample and separated using the Vanquish Neo UHPLC system, operated by the Neo UHPLC chromatography system from Thermo Scientific. The MS data from all samples were then merged using the DIA-NN software to conduct a database search of DIA MS data and perform protein DIA quantitative analysis. The database used was UniProtKB-Colletotrichum gloeosporioides [474922]-33134-20240511.fasta, obtained from the website <https://www.uniprot.org/taxonomy/474922>. Finally, a statistical analysis of the DIA protein quantitative results data was conducted. Proteins that met the criteria of a fold change greater than 1.5-fold (up/down) and a P-value less than 0.05 were considered significant differentially expressed proteins.

2.12. Statistical analysis

The data were analyzed using Origin 2021 and GraphPad Prism 9.5.0 by one-way analysis of variance. The significance of the differences was assessed using the Tukey's HSD test. $P < 0.05$ indicated a significant difference.

3. Results

3.1. In vitro experiments with GP5 inhibition of *C. gloeosporioides*

The mycelial growth inhibition caused by compounds GP4-GP7 was determined using the hypha growth rate method, and the corresponding results are presented in Fig. 2. As shown in Fig. 2A, compounds GP4-GP7 exhibited a significant inhibitory effect on the mycelium growth of *C. gloeosporioides* in a dose-dependent manner. The EC₅₀ of the four compounds were determined to be 96.98, 27.5, 38.48, and 61.59 mg L⁻¹ (Table S2). By considering the mycelial diameter and mycelial inhibition rate (Fig. 2B, C), it was evident that GP5 had the most favorable effect among the four compounds investigated. When GP5 was at a concentration of 12.5 mg L⁻¹, it exhibited a significantly higher efficacy against *C. gloeosporioides* compared to other gypenosides compounds. At

a concentration of 25 mg L⁻¹, GP5 achieved an inhibition of *C. gloeosporioides* approached 50 %. Additionally, the antifungal efficacy of the four compounds surpassed that of both the chemical pesticide chlorothalonil and the plant-derived pesticide matrine.

3.2. Spore germination

The effect of GP5 on spore germination and elongation of bud tube was investigated through microscopic observation, and the results were shown in Fig. 3. Spore cultured for 6 h initiated germination without GP5 treatment, but no germination was observed at GP5 concentrations of EC₅₀ and 400 mg L⁻¹. After 8 h of spore culture, it was observed that the spore of *C. gloeosporioides* germinated at an EC₅₀ concentration, and the longest length of the bud tube in the blank control group was measured to be 32.72 µm. After a 10 h culture of spore, the spore remained ungerminated at a concentration of 400 mg L⁻¹ for GP5. When the GP5 concentration reached the EC₅₀, the length of the spore bud tube was 11.11 µm, while the length of the spore bud tube in the blank control had already reached 92.70 µm. Therefore, the GP5 was able to significantly inhibit the elongation of the spore bud tube at EC₅₀, and it also inhibited spore germination at a concentration of 400 mg L⁻¹.

3.3. In vivo experiments with GP5 inhibition of *C. gloeosporioides*

As depicted in Fig. 4, GP5 has been shown to effectively inhibit the diameter of anthrax lesions in apples, grapes, and tomatoes. When the concentration of GP5 administration reached 500 mg L⁻¹, the incidence of anthrax in apples, grapes, and tomatoes can be significantly suppressed. In the case of apple anthrax disease at a concentration of 1000 mg L⁻¹, the incidence was reduced by 100 % after 9 d of culture compared to the control group, and by 77.52 % after 12 d of culture. Treatment with GP5 at a concentration of 1000 mg L⁻¹ could inhibit the incidence of grape anthrax after 4 d of culture, and tomato anthrax after 11 d of culture.

3.4. Mycelial morphology and intracellular structural changes

After observing the mycelial morphology using a scanning electron microscope (Fig. 5A₁-A₃), it was observed that the control group without GP5 exhibited full and intact mycelial, while the GP5-treated mycelial appeared partially desiccated. Furthermore, at a GP5 concentration of 400 mg L⁻¹, GP5 was found to potentially affect cell wall structure and induce enhanced cell wall adhesion, which warrants further investigation.

To further investigate the impact of GP5 on the cellular structure of *C. gloeosporioides*, changed in intracellular structure were examined using TEM. As depicted in Fig. 5B, B₁-B₂ represented the control cell structure, where cells without GP5 treatment displayed thick, well-defined cell walls and well-structured intracellular organelles. B₃-B₄ illustrated the intracellular structure of cells treated with the EC₅₀ concentration of GP5. In this state, the mitochondrial structure became blurred, the mitochondrial cristae break, and the organelle structure became unrecognizable. B₅-B₆ demonstrated the effects of cells treated with GP5 at a concentration of 400 mg L⁻¹. It was evident that autolysosomes appeared within the cell, indicating the occurrence of autophagy, and the organelle structure became indistinguishable. Therefore, it was hypothesized that GP5 could induce cell death by triggering cell autophagy, thereby exerting an antifungal effect.

3.5. Autophagy-related assays

As depicted in Fig. 6, the images in Fig. 6A represented the outcomes of the control group following AO treatment, as observed through a fluorescence microscope. Only green fluorescence was observed, with no presence of red fluorescence, indicating that there was no significant

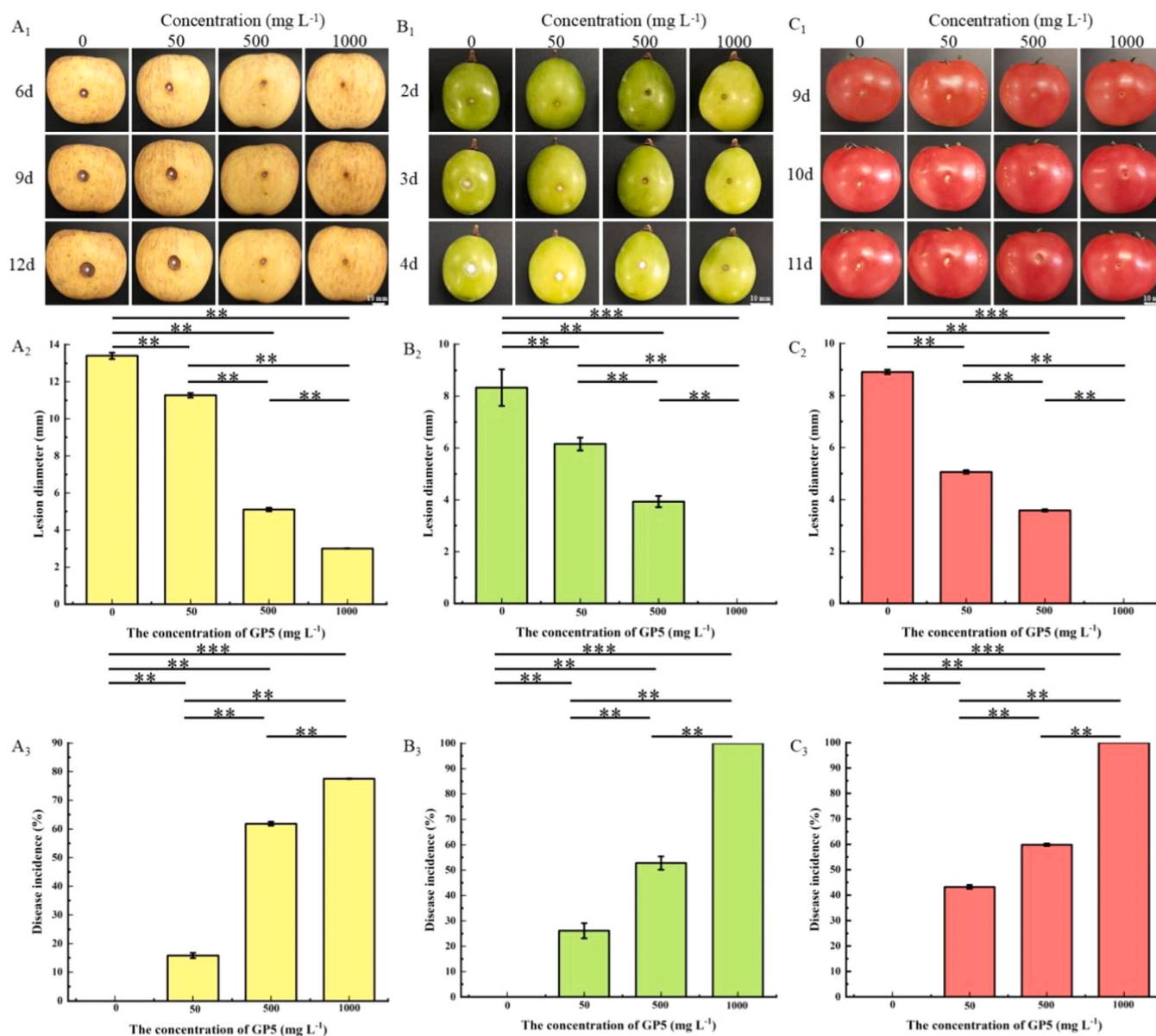


Fig. 4. GP5 inhibits *C. gloeosporioides* virulence on harvested fruit. (A₁) Lesion development on harvested apple. (A₂, A₃) Histograms for statistical data on an apple and inhibition ratio lesion. (B₁) Lesion development on harvested grapes. (B₂, B₃) Histograms for statistical data on lesion on grapes and inhibition ratio. (C₁) Lesion development on harvested tomato. (C₂, C₃) Histograms for statistical data on a tomato and inhibition ratio lesion. Vertical bars represent standard deviations of the means, n=5. Asterisks denote significant differences, ** $P < 0.01$, *** $P < 0.001$.

occurrence of autophagy in the cells under normal culture conditions. Conversely, after GP5 treatment, a substantial amount of red fluorescence was observed through AO staining under a fluorescence microscope (Fig. 6B), suggesting the presence of numerous acidic vesicle cell structures within the cells. These structures corresponded to a large number of autophagosomes and lysosomes, indicating the occurrence of autophagy in the cells. This finding aligned with the previous observations made through TEM.

3.6. Detection of the intracellular Ca²⁺ concentration

The change in intracellular Ca²⁺ concentration was depicted in Fig. 7. The distribution of Ca²⁺ in the mycelial cells without GP5 treatment extended throughout the mycelium. In Fig. 7B₂, the intracellular calcium in GP5 cells was observed to have a punctate distribution, with slightly stronger fluorescence brightness compared to the control cells. This suggested that the calcium content was enhanced after

GP5 treatment. Consequently, we hypothesized that the number of Ca²⁺ in the GP5-treated cells was elevated, leading to the regulation of the cells themselves and the occurrence of autophagy.

3.7. Mitochondrial membrane potential detection

From the transmission electron microscopy map, it was evident that GP5 caused structural damage in the cell. To assess the impact of GP5 on mitochondria, fluorescence microscopy was conducted using JC-1 staining. The results were presented in Fig. 8. Fig. 8A illustrated the control group without GP5 treatment, displaying a strong red color when exposed to green excitation light and no green color when exposed to blue excitation light. Mycelium observed under the treatment of EC₅₀ concentration exhibited a decrease in red fluorescence and an increase in green fluorescence, as observed using a fluorescence microscope (Fig. 8B). When the GP5 concentration was increased to 400 mg L⁻¹, the mycelial red fluorescence was weak, and the green fluorescence

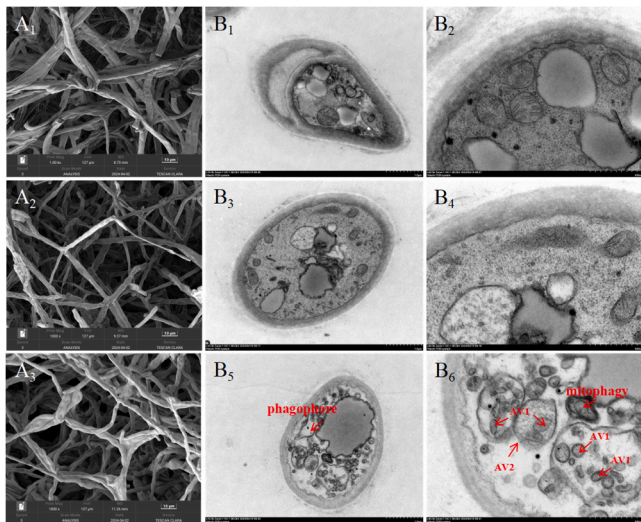


Fig. 5. Electron microscopic observation after GP5 treatment. (A) mycelial status as observed under SEM. A₁ is the control group, A₂ is the treated *C. gloeosporioides* at the EC₅₀ concentration, and A₃ is the 400 mg L⁻¹ GP5 treated *C. gloeosporioides*. (B) Intracellular structures were observed under TEM. B₁-B₂ is control, B₃-B₄ is cells treated at EC₅₀ concentration, and B₅-B₆ is cells treated with 400 mg L⁻¹ GP5. AV1: autophagosome, AV2: autolysosome.

intensity was significantly enhanced (Fig. 8 C₃) compared to the control (Fig. 8 A₃). Therefore, as the concentration of GP5 increased, the red fluorescence intensity gradually weakened, and the green fluorescence intensity gradually increased. This finding demonstrated that the concentration of GP5 was inversely proportional to the mitochondrial membrane potential, suggesting that GP5 has the ability to induce mitochondrial membrane damage, disrupt mitochondrial function, and trigger mitophagy.

3.8. Proteomic analysis

To comprehend the alterations in protein expression of the *C. gloeosporioides* following GP5 treatment and gained a more profound understanding of how GP5 induces autophagy through protein regulation, the findings were presented in Fig. 9. A total of 271 proteins exhibited differential expression compared to the control group, with 214 proteins being up-regulated and 57 proteins being downregulated (Fig. 9A). A circular heatmap (Fig. 9B) illustrated the differential proteins between the control group and the experimental group. It was observed that certain differential proteins exhibited similar functions, participated in the same biological pathways, or were located in adjacent regulatory positions within the pathway. Consequently, additional analysis was necessary for these differential proteins.

Firstly, the analysis of differential proteins (DEPs) GO function (Fig. 9C) indicated that DEPs were primarily involved in metabolic processes and cellular processes in the biological process (BP). In the

analysis of cell components (CC), DEPs were mainly concentrated in cell anatomical entities and protein complexes. In the analysis of molecular function (MF), different genes primarily focused on catalytic activity and binding. A comprehensive analysis and examination of the aforementioned functional annotations indicated that the enriched bubble map of the three branches within the top 10 significant findings (Fig. 9D) demonstrated that the differential proteins were particularly significant in the processes of organic substance metabolism, cellular nitrogen compound metabolism, and gene expression.

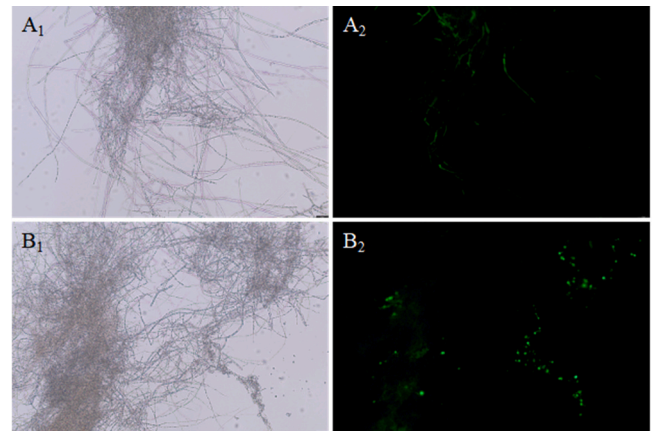


Fig. 7. Changes in the intracellular Ca²⁺ concentration. (A) Control group (without GP5 treatment). (B) Fluorimetry, AM staining fluorescence after treatment with GP5 at 400 mg L⁻¹.

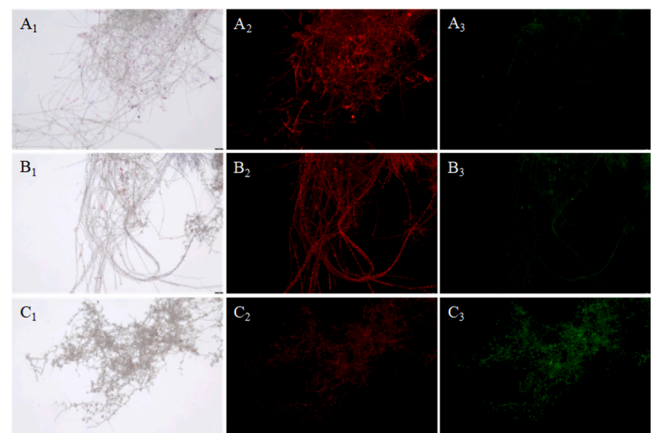


Fig. 8. Mitochondrial membrane potential changes after GP5 treatment changed in *C. gloeosporioides* treated with GP5. (A) Control group (without GP5 treatment). (B) Sustained by JC-1 after GP5 treatment at EC₅₀ concentration. (C) JC-1 staining fluorescence after treatment with GP5 at 400 mg L⁻¹.

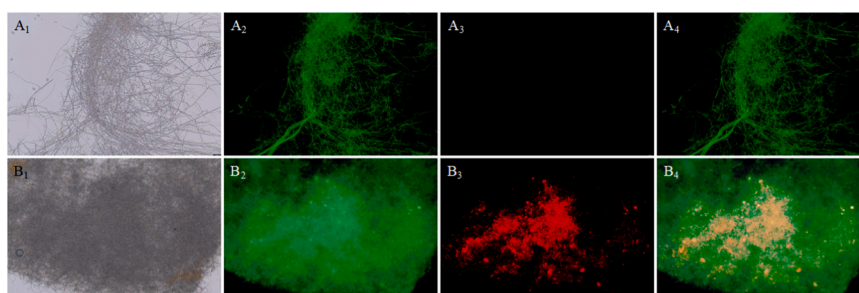


Fig. 6. AO staining after GP5 treatment. (A) Control (without GP5 treatment). (B) *C. gloeosporioides* treated with 400 mg L⁻¹ GP5.

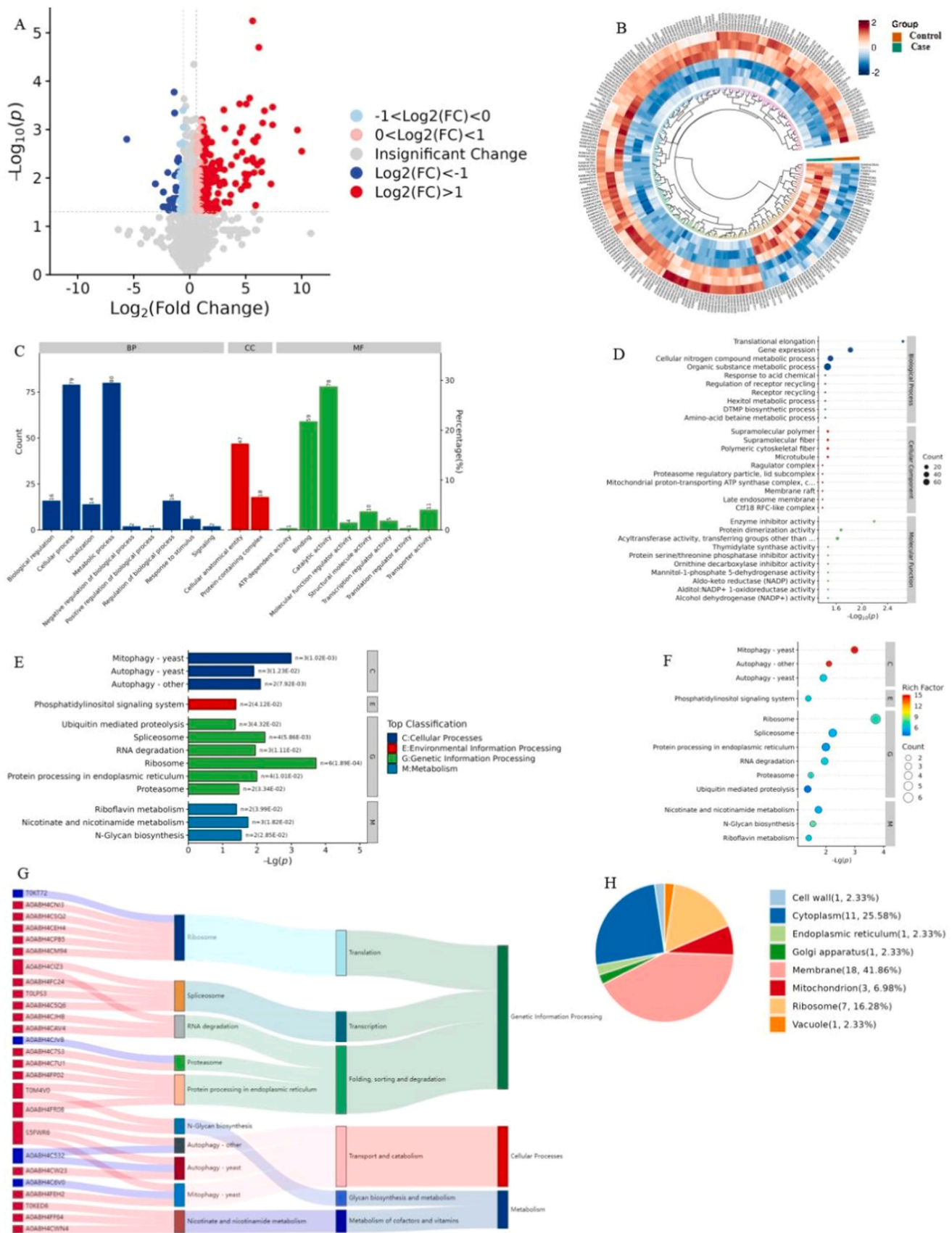


Fig. 9. Proteomics data analysis. (A) Volcano plot of the differential proteins. (B) Annular heat map of the differential protein. (C) Bar chart of GO analysis. (D) Significance of DEPs enrichment under top 10 terms of BP, MF, and CC. (E) Bar chart of KEGG pathway with significant top30 for DEPs pathway enrichment. (F) Bubble plot of the pathway with DEPs pathway enrichment significant top 30, circle size for count, color for rich factor. (G) Sankey diagram of the relationship between DEPs and pathways for the top 10 pathways.

The DEPs underwent KEGG pathway analysis, which revealed the significant top 30 pathways enriched with DEPs, as shown in Fig. 9E. The DEPs primarily focused on genetic information processing, including the ribosome, spliceosome, and ubiquitin-mediated proteins. Among these, the DEPs in cellular process pathways were mainly enriched in autophagy processes, such as mitophagy. Additionally, the KEGG pathway analysis indicated that the top 30 differentially enriched protein pathways were represented as an enrichment factor (Fig. 9F). It was observed that the circle representing mitochondrial autophagy and autophagy exhibited the deepest color, indicating a higher enrichment factor and thus a more reliable enrichment of DEPs in this pathway. To gain a deeper understanding of the relationship between the DEPs and each pathway, a Sankey diagram was created to illustrate the relationship between the top 15 differential proteins and the pathways (Fig. 9G). Five differential proteins associated with autophagy were identified: Autophagy-related protein Atg8 (k08341), Phosphatidylinositol 3-kinase Vps34 (k00914), Vacuolar amino acid transporter 3 (k14209), Transcriptional regulatory protein Sin3 (k11644), and Wsc domain-containing protein (k11244). Among these, Vps34 and Wsc proteins were downregulated, while the remaining proteins were up-regulated.

To comprehend the alterations in organelle-associated proteins, an analysis was conducted to determine the subcellular localization of the differential proteins, as illustrated in Fig. 9H. A minor extracellular protease, Vpr (A0A8H4CRF1), was identified as a differential protein associated with the cell wall. This protein was upregulated after treatment with GP5. The proteins associated with the vacuole include the late endosomal/lysosomal adaptor and MAPK and mTOR activator-domain-containing protein (LAMTOR) (A0A8H4C5A4). The expression of this protein was down-regulated. There were three proteins associated with mitochondria, namely the mitochondrial pyruvate carrier (MPC) (A0A8H4FH76), cytochrome C oxidase assembly protein Cox16 (A0A8H8WNM6), and an uncharacterized protein. The expression of MPC and Cox16 was found to be downregulated.

4. Discussion

Anthrax is recognized as one of the major plant diseases worldwide, ranking eighth in terms of prevalence and affecting a wide range of host plants (Diao et al., 2017; Rockenbach et al., 2015; Wang et al., 2017a). Currently, chemical drugs are the primary methods used for prevention and control. However, the excessive use of these drugs leads to environmental pollution and compromises food safety. Consequently, there is a growing interest among researchers in exploring plant-derived pesticides as an alternative. Among these, matrine, ostiole, and d-limonene have been identified as effective plant-derived pesticides against anthrax. In this study, it was discovered that four gypenosides (GP4-GP7) exhibited significant anti-*C. gloeosporioides* activity, surpassing the antifungal activity of matrine. To our knowledge, this was the first report on the activity of dammarane-type saponins against *C. gloeosporioides*. Furthermore, according to the inhibitory effect of the compounds GP4-GP7 on *C. gloeosporioides*, the preliminary structure-activity relationships (SARs) were summarized as follows: (1) The activities of the compounds possessing one acetyl group attached at C-6' were superior to those of the other compounds (by comparing GP4 and GP5, GP6 and GP7, respectively). (2) The C-23 configuration had a subtle impact on biological activity, but there was no definite regularity (by comparing GP4 and GP7, GP5 and GP6, respectively).

In this study, the primary mechanism of GP5 antifungal action was determined to be the induction of autophagy. Autophagy is a normal dynamic process in which cells use lysosomal degradation to selectively remove damaged, aging, or excess biological macromolecules and organelles, and release free small molecules for cell recycling (Pollack et al., 2009). Autophagy is considered a self-protective mechanism in organisms and consists of three types: microautophagy, macroautophagy, and chaperone-mediated autophagy (Zhou et al., 2022). Mitophagy is a selective autophagy process that specifically clears

dysfunctional mitochondria from the cytosol, thereby maintaining the integrity of mitochondrial function and cellular homeostasis (Kumar and Reichert, 2021; Liu and Okamoto, 2018). However, an excessive amount of autophagy processes can lead to cellular damage and disrupt their regular life processes. Proteomics has definitively identified several proteins associated with autophagy, such as Vpr, Wsc, LAMTOR, Atg8, MPC, and Cox16.

Vpr is a serine protease that functions as an extracellular protease and has the ability to degrade proteins. The upregulation of Vpr expression may lead to proteolysis of the cell wall and cell membrane, as well as increased membrane permeability (Cheng et al., 2023; Choi et al., 2010). This facilitates the entry of GP5 into the cell membrane and affect intracellular structures. Additionally, the presence of metal ions in the external environment, such as Ca^{2+} , can more easily enter the cell. Wsc is localized to the extracellular periphery and vacuoles, and is involved in various cell wall/membrane-related and vacuolar events, including vacuolar protein sorting, cellular homeostasis, signaling, and stress responses, which are crucial for fungal adaptation to the host and environment (Tong et al., 2019). The loss of Wsc can lead to reduced Hog1 phosphorylation and activation of the Hog-MAPK pathway (Ohsawa et al., 2022), which further affects the process of autophagy. Furthermore, the loss of Wsc simultaneous results in a significant increase in cell sensitivity to osmotic, oxidation, cell wall interference stress, and metal ions such as Zn^{2+} , Mg^{2+} , Fe^{2+} , K^{+} , Ca^{2+} , and Mn^{2+} (Tong et al., 2016). Detection of intracellular Ca^{2+} concentration revealed an elevated intracellular Ca^{2+} concentration following GP5 treatment. An elevated cytoplasmic Ca^{2+} concentration can further activate AMPK, suppress mTORC, and activate the autophagy system (Bootman et al., 2018; Liu et al., 2023). LAMTOR and Atg8 are also regulatory proteins associated with autophagy. The downregulation of the protein LAMTOR, which is a novel lysosomal membrane adaptor, can impact the regulation of lysosomal activation. This downregulation allows for mTOR inhibition, leading to the activation of autophagy (Malek et al., 2012). The Atg8 protein is a ubiquitin-like protein that is also utilized as a marker for autophagy (Maeda et al., 2016). An elevation of Atg8 levels indicates that cells have entered the autophagosome stage (Trajkovic et al., 2020). MPC and Cox16 proteins, which are localized to mitochondria, are regulatory proteins associated with mitochondrial autophagy. The downregulation of MPC expression leads to a decrease in mitochondrial energy, thereby triggering the activation of mitochondrial autophagy (Zangari et al., 2020). Cox16 is primarily involved in the metallization of mitochondrial Cox2 and its assembly with Cox1. However, the downregulation of Cox16 expression affects the formation of cytochrome C oxidase and the process of oxidative phosphorylation (Aich et al., 2018). This ultimately results in a reduction in mitochondrial energy production and the occurrence of mitochondrial autophagy. Subsequently, it is responsible for synthesizing bilayer membranes that make up autophagosome vesicles. These vesicles are used to transport cargo from the cytosol to the vacuolar lumen, thereby completing the process of clearing damaged mitochondria. What is more significant is that this study directly observed the process of autophagy of mitochondria with functional and structural damage after GP5 treatment.

In this study, we have elucidated the inhibitory mechanism of gypenosides on the growth and pathogenicity of *C. gloeosporioides*. To the best of our knowledge, this is the first investigation of the mechanism of dammarane-type saponins against plant pathogenic fungi from the perspective of autophagy.

5. Conclusions

GP5 exhibited significant antifungal activity against *C. gloeosporioides* both *in vitro* and *in vivo*. We proposed that GP5 induced alterations in the expression of cell membrane proteins within the cell wall, leading to increased cell permeability. This allowed GP5 to enter the cell and results in an enrichment of Ca^{2+} in the cytoplasm, disrupting

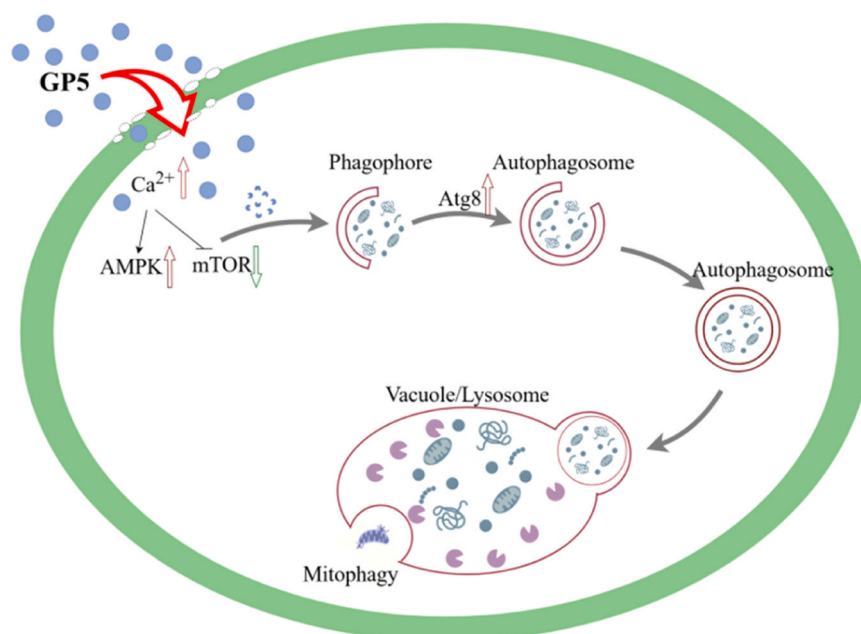


Fig. 10. The antifungal mechanism of GP5 against *C. gloeosporioides*. Thanks to Figdraw for the graphic material (<https://www.figdraw.com/>).

intracellular Ca^{2+} homeostasis. Additionally, the decreased expression of LAMTOR and Wsc triggers activation of the cellular autophagy system. The upregulation of Atg8 expression promotes the formation of autophagosomes. The downregulation of MPC and Cox16 expression promotes mitochondrial damage and autophagy. Consequently, GP5 exerted its antifungal effect by inhibiting cellular activity through activation of the autophagy system (Fig. 10). In conclusion, GP5 is a safe and effective botanical active substance that can serve as an alternative to chemical fungicides for the management of postharvest pathogens, thereby preventing and controlling anthrax in fruits and vegetables.

CRedit authorship contribution statement

Chu Gong: Funding acquisition. **Xinyv Li:** Writing – original draft, Methodology. **Yujie Liu:** Writing – original draft, Methodology, Investigation, Formal analysis, Data curation. **Jun-Li Yang:** Writing – review & editing, Supervision, Funding acquisition. **Min Han:** Writing – review & editing. **Jun Wang:** Writing – review & editing, Writing – original draft, Supervision, Methodology. **Yonghong Cao:** Funding acquisition.

Declaration of Competing Interest

The authors declare that they have no known competing financial interests or personal relationships that could have appeared to influence the work reported in this paper.

Acknowledgments

Natural Science Foundation of Shandong Province (No. ZR2023QB200), Major Science and Technology Program of Gansu Province (23ZDNA002 and 23ZYQK0001), the Scientific research Program of Longnan City (2022-S•QKJ-03 and 2022-S•QKJ-05), as well as the Scientific Research Programs of Shandong Laboratory of Advanced Materials and Green Manufacturing at Yantai (E1R03SXM04) and Yantai Development Zone Science and Technology Leading Project (2022RC005). We thank Shanghai Bioprofile Technology Company Ltd. for technical support in the proteomics experiments.

Supporting information

^{13}C NMR Data for Compounds GP4-GP7 (Table S1). Inhibition rates of the compounds at different concentrations, and EC_{50} (Table S2). ^1H and ^{13}C NMR spectra of GP4-GP7 (Figure S1-S8).

Appendix A. Supporting information

Supplementary data associated with this article can be found in the online version at [doi:10.1016/j.postharvbio.2024.113305](https://doi.org/10.1016/j.postharvbio.2024.113305).

Data availability

Data will be made available on request.

References

- Aich, A., Wang, C., Chowdhury, A., Ronsör, C., Pacheu-Grau, D., Richter-Dennerlein, R., Dennerlein, S., Rehling, P., 2018. COX16 promotes COX2 metallation and assembly during respiratory complex IV biogenesis. *eLife* 7, e32572.
- Bootman, M.D., Chehab, T., Bultynck, G., Parys, J.B., Rietdorf, K., 2018. The regulation of autophagy by calcium signals: do we have a consensus? *Cell Calcium* 70, 32–46.
- Cheng, Y., Han, J., Song, M., Zhang, S., Cao, Q., 2023. Serine peptidase Vpr forms enzymatically active fibrils outside *Bacillus bacteria* revealed by cryo-EM. *Nat. Commun.* 14 (1), 7503.
- Cheng, Z., Li, R., Jiang, Z., Tang, Y., Li, W., Shao, Y., 2022. Combined effect of *Bacillus siamensis* and chlorogenic acid on maintenance of quality and control of disease in stored wax apple fruit. *Food Qual.* 6, 1–12.
- Choi, N.-S., Chung, D.-M., Park, C.-S., Ahn, K.-H., Kim, J.S., Song, J.J., Kim, S.-H., Yoon, B.-D., Kim, M.-S., 2010. Expression and identification of a minor extracellular fibrinolytic enzyme (Vpr) from *Bacillus subtilis* KCTC 3014. *Biotechnol. Bioproc. E.* 15, 446–452.
- De Silva, D.D., Crous, P.W., Ades, P.K., Hyde, K.D., Taylor, P.W.J., 2017. Life styles of *Colletotrichum* species and implications for plant biosecurity. *Fungal Biol. Rev.* 31, 155–168.
- Dean, R., Van Kan, J.A.L., Pretorius, Z.A., Hammond-Kosack, K.E., Di Pietro, A., Spanu, P.D., Rudd, J.J., Dickman, M., Kahmann, R., Ellis, J., Foster, G.D., 2012. The Top 10 fungal pathogens in molecular plant pathology. *Mol. Plant Pathol.* 13, 414–430.
- Deng, Y.-j., Chen, Z., Chen, Y.-p., Wang, J.-p., Xiao, R.-f., Wang, X., Liu, B., Chen, M.-c., He, J., 2024. Lipopeptide C17 fengycin B exhibits a novel antifungal mechanism by triggering metacaspase-dependent apoptosis in *Fusarium oxysporum*. *J. Agric. Food Chem.* 72, 7943–7953.
- Diao, Y.Z., Zhang, C., Liu, F., Wang, W.Z., Liu, L., Cai, L., Liu, X.L., 2017. *Colletotrichum* species causing anthracnose disease of chili in China. *Pers. Mol. Phylogeny Evol. Fungi* 38, 20–37.

- Do, H.T.T., Nguyen, T.H., Nghiem, T.D., Nguyen, H.T., Choi, G.J., Ho, C.T., Le Dang, Q., 2021. Phytochemical constituents and extracts of the roots of *Scutellaria baicalensis* exhibit *in vitro* and *in vivo* control efficacy against various phytopathogenic microorganisms. *S. Afr. J. Bot.* 142, 1–11.
- Geng, Y.-N., Zhao, M., Yang, J.-L., Cheng, X., Han, Y., Wang, C.-B., Jiang, X.-F., Fan, M., Zhu, L.-L., 2022a. GP-14 protects against severe hypoxia-induced neuronal injury through the AKT and ERK pathways and its induced transcriptome profiling alteration. *Toxicol. Appl. Pharm.* 448, 116092.
- Geng, Y., Yang, J., Cheng, X., Han, Y., Yan, F., Wang, C., Jiang, X., Meng, X., Fan, M., Zhao, M., Zhu, L., 2022b. A bioactive gypenoside (GP-14) alleviates neuroinflammation and blood brain barrier (BBB) disruption by inhibiting the NF- κ B signaling pathway in a mouse high-altitude cerebral edema (HACE) model. *Int. Immunopharmacol.* 107, 108675.
- Health, E.Po.P., Bragard, C., Baptista, P., Chatzivassiliou, E., Di Serio, F., Gonthier, P., Jaques Miret, J.A., Justesen, A.F., MacLeod, A., Magnusson, C.S., Milonas, P., Navas-Cortes, J.A., Parnell, S., Potting, R., Reignault, P.L., Stefani, E., Thulke, H.H., Van der Werf, W., Vicent Civera, A., Yuen, J., Zappala, L., Migheli, Q., Vloutoglou, I., Czwienczek, E., Maiorano, A., Streissl, F., Reignault, P.L., 2022. Pest categorisation of *Colletotrichum aenigma*, *C. alienum*, *C. perseae*, *C. siamense* and *C. theobromicola*. *EFSA J.* 20, 7529.
- Hu, J., Wu, J., Wang, M., Jiao, W., Chen, Q., Du, Y., Chen, X., Yang, X., Fu, M., 2023. p-coumaric acid prevents *Colletotrichum gloeosporioides* by inhibiting membrane targeting and organic acid metabolism. *Postharvest Biol. Tec.* 204, 112447.
- Kumar, R., Reichert, A.S., 2021. Common principles and specific mechanisms of mitophagy from yeast to humans. *Int. J. Mol. Sci.* 22, 4363.
- Liu, F., Ma, Z.Y., Hou, L.W., Diaio, Y.Z., Wu, W.P., Damm, U., Song, S., Cai, L., 2022. Updating species diversity of *Colletotrichum*, with a phylogenomic overview. *Stud. Mycol.* 101, 1–56.
- Liu, S., Chen, M., Wang, Y., Lei, Y., Huang, T., Zhang, Y., Lam, S.M., Li, H., Qi, S., Geng, J., Lu, K., 2023. The ER calcium channel Csg2 integrates sphingolipid metabolism with autophagy. *Nat. Commun.* 14, 3725.
- Liu, Y., Okamoto, K., 2018. The TORC1 signaling pathway regulates respiration-induced mitophagy in yeast. *Biochem. Bioph. Res. Co.* 502, 76–83.
- Lu, K.-W., Ma, Y.-S., Yu, F.-S., Huang, Y.-P., Chu, Y.-L., Wu, R.S.-C., Liao, C.-L., Chueh, F.-S., Chung, J.-G., 2017. Gypenosides induce cell death and alter gene expression in human oral cancer HSC-3 cells. *Exp. Ther. Med.* 14, 2469–2476.
- Maeda, Y., Oku, M., Sakai, Y., 2016. Autophagy-independent function of Atg8 in lipid droplet dynamics in yeast. *J. Biochem.* 161, 339–348.
- Malek, M., Guillaumot, P., Huber, A.L., Lebeau, J., Pétrilli, V., Kfoury, A., Mikaelian, I., Renno, T., Manié, S.N., 2012. LAMTOR1 depletion induces p53-dependent apoptosis via aberrant lysosomal activation. *Cell Death Dis.* 3 e300–e300.
- Ohsawa, S., Oku, M., Yurimoto, H., Sakai, Y., 2022. Regulation of peroxisome homeostasis by post-translational modification in the methylotrophic yeast *Komagataella phaffii*. *Front. Cell Dev. Biol.* 10, 887806.
- Pollack, J., Harris, S., Marten, M., 2009. Autophagy in filamentous fungi. *Fungal Genet. Biol.* 46, 1–8.
- Qiao, Y., Xu, L., Xu, G., Cao, Y., Gao, Y., Wang, Y., Feng, J., 2022. Efficacy and potential mechanism of hinokitiol against postharvest anthracnose of banana caused by *Colletotrichum musae*. *Lwt* 161, 113334.
- Rockenbach, M.F., Boneti, J.I., Cangahuala-Inocente, G.C., Gavioli-Nascimento, M.C.A., Guerra, M.P., 2015. Histological and proteomics analysis of apple defense responses to the development of *Colletotrichum gloeosporioides* on leaves. *Physiol. Mol. Plant P.* 89, 97–107.
- Tong, S.M., Chen, Y., Zhu, J., Ying, S.H., Feng, M.G., 2016. Subcellular localization of five singular WSC domain-containing proteins and their roles in *Beauveria bassiana* responses to stress cues and metal ions. *Environ. Microbiol. Rep.* 8, 295–304.
- Tong, S.M., Wang, D.Y., Gao, B.J., Ying, S.H., Feng, M.G., 2019. The DUF1996 and WSC domain-containing protein Wsc11 acts as a novel sensor of multiple stress cues in *Beauveria bassiana*. *Cell. Microbiol.* 21, e13100.
- Trajkovic, V., Roberto, T.N., Lima, R.F., Pascon, R.C., Idrum, A., Vallim, M.A., 2020. Biological functions of the autophagy-related proteins Atg4 and Atg8 in *Cryptococcus neoformans*. *Plos One* 15, e0230981.
- Tsang, T.F., Chan, B., Tai, W.C., Huang, G., Wang, J., Li, X., Jiang, Z.H., Hsiao, W.L.W., 2019. *Gynostemma pentaphyllum* saponins induce melanogenesis and activate cAMP/PKA and Wnt/ β -catenin signaling pathways. *Phytomedicine* 60, 153008.
- Wang, C.B., Zhao, M., Wang, J., Shi, J.T., Wang, W.F., Zhang, Y., Meng, X.H., Sang, C.Y., Zhu, L.L., Yang, J.L., 2022a. Gypenosides (GPs) alleviates hypoxia-induced injury in PC12 cells and enhances tolerance to anoxia in C57BL/6 mice. *J. Food Biochem.* 46, e14448.
- Wang, C.H., Jiang, Z.T., Huang, R.J., Shi, G.C., Wang, P.P., Xue, L., 2017a. The occurrence and control to strawberry anthracnose in China. *Acta Hort.* (1156), 797–800.
- Wang, H., Yao, L., Chen, J., Ding, Z., Ou, X., Zhang, C., Zhao, J., Han, Y., 2023. Antifungal peptide P852 effectively controls *Fusarium oxysporum*, a wilt-causing fungus, by affecting the glucose metabolism and amino acid metabolism as well as damaging mitochondrial function. *J. Agric. Food Chem.* 71, 19638–19651.
- Wang, J., Li, C.-H., Farimani, M.M., Yang, J.-L., 2019. Dammarane-type saponins from *Gynostemma pentaphyllum* and their potential anti-AD activity. *Phytochem. Lett.* 31, 147–154.
- Wang, J., Meng, X.-H., Wang, W.-F., Sang, C.-Y., Ha, T.-K.-Q., Yang, J.-L., 2022b. Dammarane triterpenoids with rare skeletons from *Gynostemma pentaphyllum* and their cytotoxic activities. *Fitoterapia* 162, 105280.
- Wang, J., Yang, J.-L., Zhou, P.-P., Meng, X.-H., Shi, Y.-P., 2017b. Further new gypenosides from *jiaogulan* (*Gynostemma pentaphyllum*). *J. Agric. Food Chem.* 65, 5926–5934.
- Wang, J., Zhao, M., Cheng, X., Han, Y., Zhao, T., Fan, M., Zhu, L., Yang, J.L., 2020. Dammarane-type saponins from *Gynostemma pentaphyllum* prevent hypoxia-induced neural injury through activation of ERK, Akt, and CREB pathways. *J. Agric. Food Chem.* 68, 193–205.
- Wang, K., Qin, Z., Wu, S., Zhao, P., Zhen, C., Gao, H., 2021. Antifungal mechanism of volatile organic compounds produced by *Bacillus subtilis* CF-3 on *Colletotrichum gloeosporioides* assessed using omics technology. *J. Agric. Food Chem.* 69, 5267–5278.
- Wu, J., Hu, J., Jiao, W., Du, Y., Han, C., Chen, Q., Chen, X., Fu, M., 2023. Inhibitory effect of ϵ -poly-L-lysine on fruit *Colletotrichum gloeosporioides* through regulating organic acid metabolism and exerting membrane-targeted antifungal activity. *Postharvest Biol. Tec.* 200, 112339.
- Xing, S.-F., Liu, L.-H., Zu, M.-L., Lin, M., Zhai, X.-F., Piao, X.-L., 2019. Inhibitory effect of damulin B from *Gynostemma pentaphyllum* on human lung cancer cells. *Planta Med.* 85, 394–405.
- Yang, X., Wang, Y., Jiang, H., Song, R., Liu, Y., Guo, H., Meng, D., 2023. Antimicrobial peptide CB-M exhibits direct antifungal activity against *Botrytis cinerea* and induces disease resistance to gray mold in cherry tomato fruit. *Postharvest Biol. Tec.* 196, 112184.
- Yang, Y., Xie, P., Nan, Y., Yuan, J., Gong, D., Li, Y., ... & Prusky, D.B., 2024. The low-affinity calcium channel protein AaFig1 is essential for the growth and development, infection structure differentiation, and pathogenicity of *Alternaria alternata*. *Postharvest Biol. Tec.* 210, 112756.
- Yu, H., Shi, L., Qi, G., Zhao, S., Gao, Y., Li, Y., 2016. Gypenoside protects cardiomyocytes against ischemia-reperfusion injury via the inhibition of mitogen-activated protein kinase mediated nuclear factor Kappa B pathway *in vitro* and *in vivo*. *Front. Pharmacol.* 7, 148/141-148/111.
- Zangari, J., Petrelli, F., Maillot, B., Martinou, J.-C., 2020. The multifaceted pyruvate metabolism: role of the mitochondrial pyruvate carrier. *Biomolecules* 10, 1068.
- Zhai, X.-F., Zu, M.-L., Wang, Y.-R., Cui, W.-Y., Duan, Y., Yang, C., Piao, X.-L., 2021. Protective effects of four new saponins from *Gynostemma pentaphyllum* against hydrogen peroxide-induced neurotoxicity in SH-SY5Y cells. *Bioorg. Chem.* 106, 104470.
- Zhang, S., Wang, J., Sun, H., Yang, J., Zhao, J., Wang, Y., 2023a. Inhibitory effects of hinokitiol on the development and pathogenicity of *Colletotrichum gloeosporioides*. *World J. Microb. Biot.* 39, 356.
- Zhang, X., Li, G., Zhang, Z., Tian, S., 2023b. 3-Octanol controls gray mold on postharvest fruit by inducing autophagy of *Botrytis cinerea*. *Postharvest Biol. Tec.* 205, 112525.
- Zhang, X.S., Zhao, C., Tang, W.Z., Wu, X.J., Zhao, Y.Q., 2015. Gypensapogenin H, a novel dammarane-type triterpene induces cell cycle arrest and apoptosis on prostate cancer cells. *Steroids* 104, 276–283.
- Zhou, Y., Manghwar, H., Hu, W., Liu, F., 2022. Degradation mechanism of autophagy-related proteins and research progress. *Int. J. Mol. Sci.* 23, 7301.